Journal Pre-proof

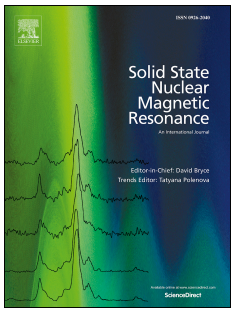

Experimental and Computational ^{17}O Solid-State NMR Investigation of Na- and K-(Bi)carbonate Salts

Austin Peach, Nicolas Fabregue, David Gajan, Frédéric Mentink-Vigier, Faith Scott, Christel Gervais, Danielle Laurencin

PII: S0926-2040(25)00036-0

DOI: https://doi.org/10.1016/j.ssnmr.2025.102020

Reference: YSNMR 102020

To appear in: *Solid State Nuclear Magnetic Resonance*

Received Date: 16 May 2025

Revised Date: 9 July 2025

Accepted Date: 10 July 2025

Please cite this article as: A. Peach, N. Fabregue, D. Gajan, F. Mentink-Vigier, F. Scott, C. Gervais, D. Laurencin, Experimental and Computational ^{17}O Solid-State NMR Investigation of Na- and K-(Bi)carbonate Salts , *Solid State Nuclear Magnetic Resonance*, https://doi.org/10.1016/j.ssnmr.2025.102020.

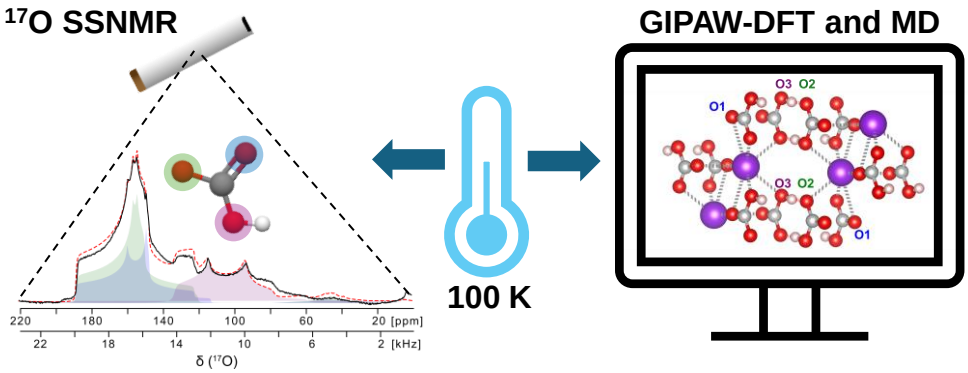

Experimental ultra-low temperature ^{17}O SSNMR analyses are combined with GIPAW-DFT and MD simulations to study oxygen environments in Na- and K-(bi)carbonate salts.

Experimental and Computational ^{17}O Solid-State NMR Investigation of Na- and K-(Bi)carbonate Salts

Austin Peach,[1,*] Nicolas Fabregue,[1] David Gajan,[2] Frédéric Mentink-Vigier,[3] Faith Scott,[3] Christel Gervais,[4] Danielle Laurencin[1,*]

1. ICGM, Univ Montpellier, CNRS, ENSCM, Montpellier, France

2. CRMN Lyon, UMR 5082 (CNRS, ENS Lyon, Université Lyon 1), Villeurbanne, France

3. National High Magnetic Field Laboratory (NHMFL), Tallahassee, Florida, USA

4. LCMCP, UMR 7574, Sorbonne Université, CNRS, Paris, France

To whom correspondence should be addressed:

austin.peach@umontpellier.fr

danielle.laurencin@umontpellier.fr

Abstract

The importance of (bi)carbonate salts cannot be understated. They are vital to the Earth's geology and ecosystems and are used as precursors by chemists for the synthesis of functional materials. Naturally, solid-state NMR (ssNMR) appears as the spectroscopic tool of choice to probe the atomic-level structure and dynamics of (bi)carbonate salts. Of the possible nuclei available as spectroscopic probes in carbonate and bicarbonate ions (*i.e.*, ^{1}H, ^{13}C, and ^{17}O), oxygen-17 is highly attractive. Yet, it is seldom employed, largely due to its low natural abundance (0.04%) and lack of practical enrichment protocols. Recently, we reported an effective ^{17}O-labeling strategy involving mechanochemistry of $Na_2CO_3{\cdot}H_2O$, Na_2CO_3, $NaHCO_3$, $K_2CO_3{\cdot}1.5H_2O$, and $KHCO_3$, and recorded their ^{17}O NMR spectral fingerprints near room temperature. In this work, ultra-low temperature (*i.e.*, 100 K) ^{17}O ssNMR spectra of these phases are acquired at two magnetic fields, 14.1 and 18.8 T, to extract the ^{17}O NMR parameters δ_{iso}, C_Q, and η_Q for the different oxygen sites, and to further study the influence of dynamics on the spectra. We compare the experimental ^{17}O NMR parameters to those computed with GIPAW-DFT calculations both on static models, and after averaging by molecular dynamics (MD) simulations. This approach was taken to aid in analyzing the structure-spectra relationships and shed light on the dynamics. Lastly, we report the static GIPAW-DFT calculations of ^{17}O NMR parameters for a series of other carbonate salts of interest, further expanding upon current experimental ^{17}O ssNMR results.

Introduction

Carbonate and bicarbonate salts are widely distributed minerals in the Earth's crust,[1] where they are found in structures involving light-weight metal ions (*e.g.,* in calcite, dolomite and trona), and/or transition metal ions (*e.g.,* in siderite and rhodochrosite). In synthetic chemistry, (bi)carbonate salts are also key precursors for the preparation of organic molecules and functional materials.[2–6] For example, $NaHCO_3$ can be used as a carbonate source in the synthesis of bone-related biomaterials (carbonated biomimetic hydroxyapatites),[7] while vaterite, the least stable polymorph of $CaCO_3$, has been employed as a reactant for the preparation of bone cements.[8]

In order to be able to fully rationalize the properties of (bi)carbonate-containing materials, it is important to be able to describe their structure at the atomic level. In this context, solid-state NMR (ssNMR) spectroscopy is invaluable. Indeed, carbonate (CO_3^{2-}) and bicarbonate (HCO_3^-) ions contain three nuclei which can potentially be analyzed by ssNMR: ^{13}C, ^{17}O, and, in the case of bicarbonates, ^{1}H (or ^{2}H). Numerous studies have reported the ^{13}C (and ^{1}H) ssNMR characterization of (bi)carbonate ions in materials,[9–12] including in phases developed for healthcare or environmental applications.[11,13–15] In contrast, because of its very low natural abundance (0.04 %) and quadrupolar nature (I = 5/2), ^{17}O ssNMR characterizations of (bi)carbonates have only gained traction over the last decade.[9,15–20]

Considering that oxygen-17 has been shown to be highly sensitive to subtle changes in its local environment,[21–23] we have been interested in improving the sensitivity of ^{17}O NMR, through the development of cost- and time-efficient ^{17}O-labeling strategies using mechanochemistry.[24–28] In a recent report, we demonstrated for the first time that this synthetic approach could be used to enrich the following Na- and K-(bi)carbonate salts: $NaHCO_3$, $Na_2CO_3{\cdot}H_2O$, Na_2CO_3, $KHCO_3$, and $K_2CO_3{\cdot}1.5H_2O$.[9] Thanks to this labeling, rapid acquisition of *high-resolution* ^{17}O NMR spectra of these phases were recorded near ambient temperature, revealing not only distinct signatures, but also suggesting the presence of molecular-level dynamics.

Herein, to further explore the influence of dynamics on the ^{17}O ssNMR signatures of the aforementioned ^{17}O-enriched Na- and K-(bi)carbonate salts, we report an ultra-low temperature ^{17}O ssNMR study of these phases. Analyses were performed at two magnetic fields, 14.1 and 18.8 T, and the ^{17}O NMR parameters (*i.e.*, δ_{iso}, C_Q, and η_Q) obtained from these spectra were first compared to those computed from static GIPAW-DFT calculations. This analysis showed

that although these calculations can provide some guidelines to help interpret the data, discrepancies remain when comparing to the experimental values. Molecular dynamics (MD) simulations were thus used, to try to help shed light on the impact local motions have on the NMR parameters, especially for the hydrated structures of $Na_2CO_3 \cdot H_2O$ and $K_2CO_3 \cdot 1.5H_2O$ (for which the assignment of the experimental ^{17}O NMR resonances is more challenging). Finally, we report static DFT calculations on a series of other simple carbonate salts of interest, further expanding upon the current experimental/computational trends. This combination of experimental ssNMR and GIPAW-DFT computations (involving both static and MD calculations of ^{17}O NMR parameters) lays a foundation for future NMR crystallographic analyses of (bi)carbonate salts and related functional materials.

Experimental details

Materials

All ^{17}O-labeled materials studied herein were mechanochemically synthesized and enriched in-house, following our previously published procedure.[9]

^{17}O Solid-State NMR

Ultra-low temperature (*i.e.*, 100 K) ^{17}O ssNMR spectra were recorded under Magic angle spinning (MAS), at two NMR facilities: the CRMN Lyon in Villeurbanne (B_0 = 18.8 T, 800 MHz instrument) and the National High Magnetic Field Lab (NHMFL) in Tallahassee (B_0 = 14.1 T, 600 MHz instrument). A double frequency sweep (DFS) was applied to enhance the sensitivity of ^{17}O MAS NMR spectra by a factor of *ca*. 2 to 3 fold.[29,30] For samples containing protons, SPINAL-64 ^{1}H decoupling was applied during acquisition, using a radio frequency of 75 to 100 kHz.[31,32] ^{17}O chemical shifts were referenced directly to tap water at δ_{iso} = 0.0 ppm.

Experiments at the NHMFL were conducted at 14.1 T [$\nu_0(^1H)$ = 600.486 MHz and $\nu_0(^{17}O)$ = 81.405 MHz]. ^{17}O MAS NMR spectra were recorded on a Bruker Avance NEO spectrometer using a custom-built low-temperature 3.2 mm HXY MAS-DNP probe with samples packed into 3.2 mm outer diameter (o.d.) sapphire rotors with Vespel drive caps. Samples were spun at a rate of 10 or 11 kHz with the sample temperature estimated to be 105 K. Spectra were acquired using a DFS-enhanced Hahn echo pulse sequence, with a CT-selective $\pi/2$ pulse of 2 μs, a π pulse of 4 μs, and an echo delay of one rotor period. Further experimental acquisition parameters can be found in the electronic supporting information (ESI), **Table S1**.

Experiments at the CRMN Lyon were conducted at 18.8 T [$\nu_0(^1H)$ = 799.700 MHz and $\nu_0(^{17}O)$ = 108.411 MHz]. ^{17}O MAS NMR spectra were recorded on an Avance NEO spectrometer using a 3.2 mm triple-resonance HXY ultra-low temperature DNP Bruker probe. Samples were packed into 3.2 mm o.d. zirconia rotors with Vespel drive tips, and spun to 12 kHz, with the sample temperature estimated to be *ca.* 105 K. Spectra were acquired using a DFS-enhanced Bloch decay (one pulse) or Hahn echo pulse sequence, with a CT-selective π/2 pulse of 2.8 μs, followed in the case of the echo by a π pulse of 5.6 μs (with an echo delay of one rotor period). A 2D multiple-quantum MAS (MQMAS) spectrum of Na_2CO_3 was also acquired using a 3Q z-filtered pulse sequence with excitation and conversion pulses of 2.3 μs and 6.5 μs, respectively, followed by a 40 μs soft pulse.[33,34] Further experimental acquisition parameters can be found in the ESI, **Tables S2** and **S3**, respectively.

Complementary ^{17}O MAS NMR experiments were conducted on anhydrous Na_2CO_3 at 14.1 T [$\nu_0(^1H)$ = 599.764 MHz and $\nu_0(^{17}O)$ = 81.307 MHz] at the ICGM (Montpellier, France). ^{17}O MAS NMR spectra were recorded on a Varian VNMRS spectrometer using a 3.2 mm triple-resonance HXY Varian probe. Samples were packed into 3.2 mm o.d. zirconia rotors with Torlon drive tips and caps, and spun at 16 kHz. The 1D ^{17}O MAS NMR spectra were acquired using a "one pulse" sequence, with a π/2 solid pulse of 2 μs. Analyses were done at two temperatures (corresponding to sample temperatures estimated to be 260 K and 315 K). A 2D MQMAS spectrum of Na_2CO_3 was also acquired using a 3Q z-filtered pulse sequence with excitation and conversion pulses of 2.3 μs and 6.5 μs, respectively, followed by a 40 μs soft pulse.[33,34] Further experimental acquisition parameters for these ^{17}O MAS NMR spectra of Na_2CO_3 be found in **Tables S4** and **S5**.

All spectra were processed using the TopSpin v4.1.4 and ssnake v1.5[35] software packages. The ^{17}O NMR parameters were obtained using the quadrupolar fitting module included in ssnake and the uncertainties assessed by bidirectional variation of each parameter.

Computational Details

Plane-wave density functional theory (DFT) calculations were carried out on reported crystal structures, retrieved from the Inorganic Crystal Structure Database (ICSD), of the following metal carbonate salts: Na_2CO_3,[36] $Na_2CO_3{\cdot}H_2O$,[37] $NaHCO_3$,[38] K_2CO_3 (γ phase),[39] $K_2CO_3{\cdot}1.5H_2O$,[40] $KHCO_3$,[41] $CaCO_3$ (calcite),[42] $MgCO_3$,[43] Li_2CO_3,[44] and $ZnCO_3$.[43]

The Vienna *ab initio* simulation package (VASP)[45–47] was used to carry out geometry optimizations. The revised Perdew-Burke-Erzenhof (rPBE)[48] generalized gradient approximation (GGA) functional was employed, with an energy cut-off of 400 eV, a Monkhorst-Pack k-space grid size chosen to obtain a unit cell with cubic symmetry, and using Grimme's D3 dispersion correction.[49] The dimensions of the unit cell were kept fixed for both H-atom (H Rel) and all atom (All Rel) geometry optimizations.

Oxygen-17 chemical shieldings and quadrupolar NMR parameters (*i.e.*, C_Q and η_Q) were computed for both unrelaxed and VASP geometry optimized structures, using the QUANTUM-ESPRESSO (QE) software package.[50] The NMR parameters were computed using the GIPAW[51] approach, with the PBE[52] GGA functional, norm conserving pseudopotentials in the Kleinman-Bylander form to describe the valence electrons,[53] an energy cut-off of 80 Ry, and a cubic k-space grid.

The ^{17}O quadrupolar coupling constants (C_Q) were calculated using a quadrupolar moment of –2.558 fm^2.[54] A ^{17}O magnetic shielding reference (σ_{ref}) was determined by comparing the calculated magnetic shieldings (σ_{iso}) with the experimental isotropic chemical shifts (δ_{iso}) of reported structures (**Table S6** and **Figure S1**). This σ_{ref} was then used to determine the calculated δ_{iso} where $\delta_{iso} = -(\sigma_{iso} - \sigma_{ref})$.[55] Here, σ_{ref} values of 253 and 233 ppm were used for unrelaxed and relaxed structural models, respectively. The experimental ^{17}O NMR parameters and those calculated for fully-relaxed structural models of Na- and K-(bi)carbonate salts are reported in **Table 1**.

Molecular dynamics (MD) simulations were carried out on structural models of Na- and K-(bi)carbonate salts with the CP2K code[56,57] consisting in Born-Oppenheimer MD (BOMD) with PBE electronic representation, including the Grimme (D3) correction for dispersion,[49] GTH pseudopotentials,[58] combined plane-wave, and TZVP basis sets.[59] The BOMD was performed using the NVT ensemble, and Nose–Hoover thermostat was used to control the average temperature at 100 K. Trajectories were accumulated over 15 to 90 ps, depending on the phase, with a time step of 1 fs. Calculated ^{17}O NMR parameters over the duration of the MD simulations were determined by averaging the predicted shielding and electric field gradient tensors over a set number of evenly spaced structures. For this purpose, a GIPAW calculation was performed every 500 steps for the duration of the MD (*i.e.*, 30 to 180 points for each NMR parameter). Time-averaged δ_{iso} values are the mean average of all δ_{iso} calculated for each step. The principal components of the EFG tensor for a given site were obtained by first averaging each individual components of the EFG tensor over the length of the simulation, and

then diagonalizing the averaged EFG tensor to extract principal components following the convention $|V_{33}| \geq |V_{22}| \geq |V_{11}|$. The quadrupolar interaction is then given by the values $C_Q = eQV_{33}/h$ and $\eta_Q = (V_{11} - V_{22})/V_{33}$.

2. Results and Discussion

Ultra-low temperature ^{17}O ssNMR analyses of Na- and K-(bi)carbonate salts

We recently reported and described the ^{17}O MAS NMR spectra of Na- and K-bicarbonate salts (*i.e.*, Na_2CO_3, $NaHCO_3$, $Na_2CO_3{\cdot}H_2O$, $KHCO_3$, and $K_2CO_3{\cdot}1.5H_2O$) recorded for sample temperatures ranging from 250 to 370 K.[9] Strong differences in ^{17}O lineshapes were observed (**Figure S2A**), with $NaHCO_3$ and $KHCO_3$ displaying features typical of ^{17}O second-order quadrupolar lineshapes, while the spectra of $Na_2CO_3{\cdot}H_2O$ and $K_2CO_3{\cdot}1.5H_2O$ appeared as more narrow gaussian-like signals, suggesting the interplay of molecular-level dynamics. Similarly, for Na_2CO_3, specific features of the second-order quadrupolar lineshape (*i.e.*, the presence of discontinuities) start to disappear when performing ^{17}O ssNMR analyses just above room temperature (*e.g.*, 315 K) (see **Figure S2B**). As demonstrated in previous studies on carbonates,[16,19,60] molecular-level dynamics can influence the local environments of oxygen, and, depending on their timescale, affect the ^{17}O ssNMR lineshapes, and result in a loss in resolution. Here, to try to decrease the motions, and thereby recover the second-order ^{17}O quadrupolar lineshapes of the distinct oxygen sites, ssNMR analyses of the Na- and K-(bi)carbonate salts were performed at ultra-low temperatures (close to 100 K).

Shown in **Figures 1** to **3** are the ultra-low-temperature ^{17}O ssNMR data. *All spectra* now appear with sharp discontinuities, typical of quadrupolar lineshapes. This is particularly noteworthy for $Na_2CO_3{\cdot}H_2O$ and $K_2CO_3{\cdot}1.5H_2O$, which did not show such features in our previous work (where the lowest temperature was 270 K).[9] Analyses were performed at two magnetic fields (14.1 and 18.8 T), to fit the spectra (paying special attention to spectral discontinuities), and precisely obtain the ^{17}O NMR parameters (*i.e.*, δ_{iso}, C_Q, and η_Q) of the inequivalent oxygen sites, as summarized in **Table 1**. Below, these ultra-low temperature spectra are successively discussed, by focusing only on the characterization of the CO_3^{2-}/HCO_3^- region.

Table 1: Experimental and calculated ^{17}O NMR parameters for Na- and K-(bi)carbonate salts. Values for the experimental fits are determined from analytical simulations of the ^{17}O MAS NMR spectra acquired at *ca*. 105 K at 14.1 and 18.8 T (see text for further details). The value indicated in parentheses is the experimental uncertainty in the last digit(s). DFT calculations were performed here using the GIPAW approach, on fully-relaxed structural models of each phase. Oxygen site numbers given here correspond to the atom numbers in the reported .cif files.[36–38,40,41] Experimental assignments proposed here for the two hydrates need to be taken carefully, as detailed in the last part of this manuscript.

			δ_{iso} [a] (ppm)	C_Q [b] (MHz)	η_Q [c]
Na_2CO_3 (ICSD: 168129)	O1	Exp.	162.2 (8)	7.07 (12)	0.95 (4)
		Calc.	163.8	–7.87	0.96
	O2	Exp.	161.0 (9)	6.99 (10)	0.97 (3)
		Calc.	161.7	7.99	0.99
$Na_2CO_3·H_2O$ (ICSD: 1852)	O3	Exp.	180.2 (9)	6.95 (5)	0.92 (6)
		Calc.	178.7	–7.97	0.85
	O1	Exp.	173.4 (7)	6.93 (17)	0.88 (5)
		Calc.	173.2	–7.93	0.80
	O2	Exp.	172.2 (13)	7.10 (16)	0.95 (5)
		Calc.	171.7	7.98	0.98
$NaHCO_3$ (ICSD: 18183)	O1	Exp.	174.1 (9)	7.32 (9)	0.79 (5)
		Calc.	174.7	8.17	0.88
	O2	Exp.	170.3 (9)	6.78 (7)	0.88 (2)
		Calc.	167.5	–7.83	0.75
	O3	Exp.	137.6 (8)	7.68 (7)	0.38 (3)
		Calc.	133.8	-8.50	0.46
$K_2CO_3·1.5H_2O$ (ICSD: 54765)	O1	Exp.	198.2 (7)	7.30 (7)	0.86 (6)
		Calc.	204.2	8.18	0.89
	O2	Exp.	190.7 (5)	7.07 (11)	1.00 (3)
		Calc.	193.9	–8.00	0.99
	O3	Exp.	184.9 (8)	6.90 (15)	0.87 (9)
		Calc.	183.4	–8.03	0.84
$KHCO_3$ (ICSD: 2325)	O1	Exp.	189.0 (7)	7.43 (15)	0.72 (5)
		Calc.	188.0	8.26	0.81
	O2	Exp.	187.8 (9)	6.83 (13)	0.93 (4)
		Calc.	183.3	–7.98	0.71
	O3	Exp.	136.5 (11)	7.72 (17)	0.42 (5)
		Calc.	138.8	–8.35	0.38

[a] The isotropic chemical shift, δ_{iso}, is defined as $\delta_{iso} = (\delta_{11} + \delta_{22} + \delta_{33})/3$.

[b] The quadrupolar coupling constant, C_Q, is defined as $C_Q = eQV_{33}/h$, where the principal components of the EFG tensor, V_{33}, V_{22}, and V_{11}, are defined such that $|V_{33}| \geq |V_{22}| \geq |V_{11}|$. It is not possible to determine the sign of C_Q from experimental ^{17}O NMR spectra; however, it can be determined from computation.

[c] The asymmetry parameter, η_Q, is defined as $\eta_Q = (V_{11} - V_{22})/V_{33}$.

^{17}O ssNMR of $NaHCO_3$ and $KHCO_3$

Concerning $NaHCO_3$ and $KHCO_3$, the spectra in **Figure 1** each feature up to six horns (*i.e.*, discontinuities). These are indicative of three distinct overlapping ^{17}O NMR signals, in agreement with the number of crystallographically distinct oxygen environments (denoted as O1, O2, and O3). For each phase, fits were obtained at both fields for the ^{17}O MAS lineshapes, with the corresponding NMR parameters reported in **Table 1**. These results for $NaHCO_3$ and $KHCO_3$ are fully consistent with an early 77 K ^{17}O NQR study by Cheng and Brown (see **Table S7**).[61] Here, resonances were assigned by analogy with our previously reported results,[9] which also agree with the aforementioned NQR study.

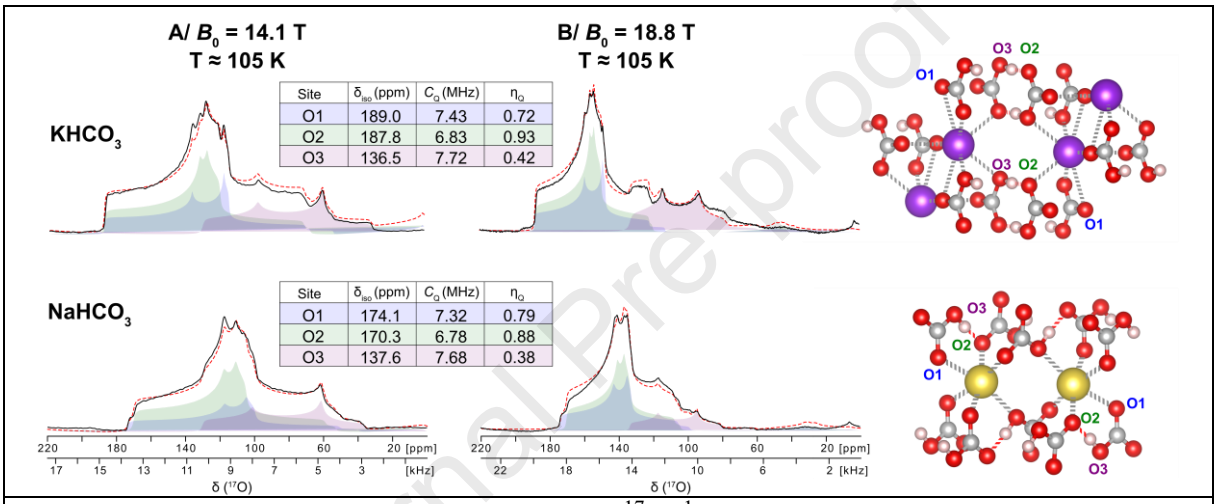

Figure 1: Experimental ultra-low temperature ^{17}O{^{1}H} MAS NMR spectra acquired at (**A**) B_0 = 14.1 T and (**B**) B_0 = 18.8 T, of ^{17}O-enriched $KHCO_3$ (top) and $NaHCO_3$ (bottom). Experimental spectra are in black and the overall fit shown in dashed red, composed of simulated fits for the three ^{17}O signals, O1, O2, and O3, in blue, green, and purple, respectively. NMR parameters are indicated in the tables (associated error bars can be found in **Table 1**). On the right, a zoomed-in view of a part of the crystal structures is shown, with the assignment of the three crystallographically distinct oxygens, which correspond to the three overlapping ^{17}O NMR signals observed in the spectra. Notably, O1 forms direct bonds with the metal ions (X···O, X = Na or K), O2 is distinguished by forming a hydrogen bond (C=O···H), and O3 is the hydroxyl oxygen (C–OH). O, C, H, Na, and K atoms are in red, grey, light pink, purple and yellow, respectively. Further details on acquisition parameters for the displayed spectra are shown in **Tables S1** and **S2**.

At this stage, several interesting observations can be made when comparing the ^{17}O NMR parameters of the two bicarbonates at 105 K to those we previously reported at 297 K (values summarized in **Table S8**). First, the δ_{iso} for the oxygen environments in $NaHCO_3$ are all within 2 ppm (for a given site). For $KHCO_3$, however, O2 and O3 (which interact through an H-bond) shift by nearly 11 ppm. Second, the values of C_Q and η_Q also change for the two samples, with notably all C_Q values increasing at low-temperature (as expected from the

reduced local motions). The most pronounced changes in quadrupolar parameters are for the C_Q and η_Q of O3 for $KHCO_3$, and for the η_Q of O2 of $NaHCO_3$ and $KHCO_3$. The latter point was already highlighted in previous NQR studies of both bicarbonates and in ssNMR studies of $KHCO_3$,[61–63] suggesting that the difference in hydrogen bonding between both structures could explain such differences. This shows how ^{17}O MAS NMR analyses at various temperatures, including ultra-low temperatures, may shed light on H-bonding within structures containing bicarbonate species.

^{17}O ssNMR of Na_2CO_3

Concerning Na_2CO_3, the ultra-low temperature 1D ^{17}O ssNMR spectra are similar to those observed at 260 K (**Figure 2** *vs.* **Figure S2B**), appearing at first glance as a single ^{17}O second-order quadrupolar lineshape. Yet, two resonances are expected based on the two inequivalent oxygen environments (with 2:1 occupancy in the crystal structure, **Table S9**). To further our analysis, a 2D ^{17}O MQMAS spectrum was acquired at 18.8 T (**Figure 2C**). In this experiment, the ^{17}O NMR signals corresponding to the different oxygen local environments can become distinguishable along the indirect (F1) dimension, in which only the isotropic components of each resonance are maintained. Here, in the ^{17}O 2D MQMAS spectrum recorded at 105 K, two signals are resolved along the F1 dimension, in a *ca.* 2:1 ratio. The relative intensity between the two signals is consistent with the crystal structure of Na_2CO_3, thus allowing the assignment of the two resonances. Individual slices were extracted along the F1 dimension (**Figure 2C**) and fitted to obtain the NMR parameters reported in **Table 1**. These values were subsequently used to fit the ultra-low temperature 1D ^{17}O NMR data (**Figure 2**), and as a starting point for the fitting of the 2D MQMAS spectra (**Figure S3**). We note that acquisition of a 2D MQMAS spectrum was also attempted at 14.1 T at a sample temperature of 250 K (**Figure S4**). However, both the field and temperature were insufficient to clearly discriminate and resolve the two overlapping sites in this case, further emphasizing the importance of acquisition conditions for high-resolution ^{17}O NMR studies of carbonate phases.

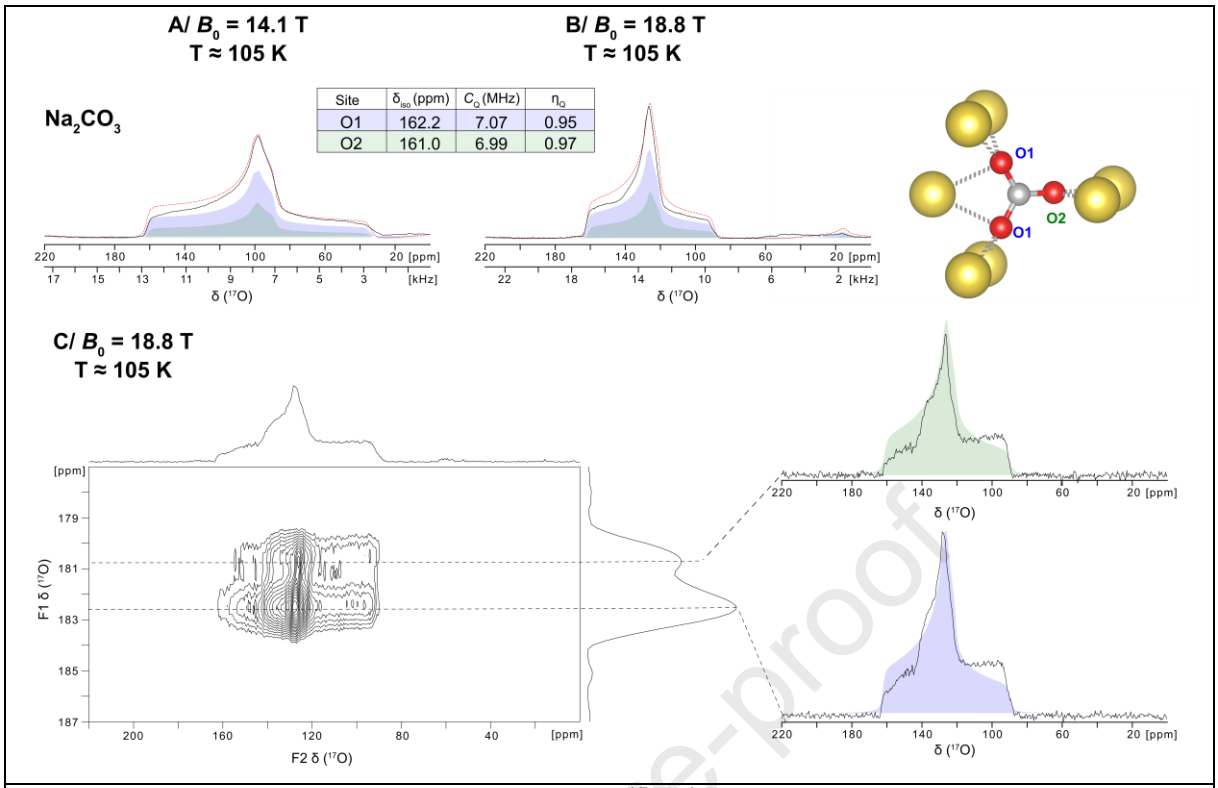

Figure 2: Experimental ultra-low temperature $^{17}O\{^1H\}$ 1D MAS NMR spectra acquired at (**A**) B_0 = 14.1 T and (**B**) B_0 = 18.8 T, and (**C**) 2D MQMAS acquired at B_0 = 18.8 T (bottom) of ^{17}O enriched Na_2CO_3. Experimental spectra are in black and the overall fit in dashed red (composed of two ^{17}O signals, O1 and O2, in blue and green, respectively, with NMR parameters as indicated in the table above, and error bars in **Table 1**). In MQMAS, two signals are resolved along the F1 dimension. Slices are extracted along the F1 dimension for the two signals and fitted accordingly, which was then used to propose a fit of the 1D spectra considering a 2:1 ratio. Further details on acquisition parameters for the displayed spectra are shown in **Tables S1** to **S3**. In the top right is a zoomed-in view of a part of the crystal structure with the assignment of the two crystallographically distinct oxygens. O, C, and Na atoms are in red, grey, and yellow, respectively. For clarity, not all Na atoms close to the oxygen sites are shown (see **Table S9** for local distances around each site).

The ^{17}O NMR parameters of the two oxygen sites (**Table 1**) are very similar, which is unsurprising considering their bonding environments in the crystal structure (**Table S9**). In both cases, aside from the C–O bond, both types of oxygens are surrounded by five Na^+ ions. The small difference of 1.2 ppm in δ_{iso} between the two sites may reflect the small variation in average Na···O bond distance, in line with the trend which had been proposed by Wong *et al.* for alkali metal oxalates.[65] Indeed, the site with the highest shift (O1) corresponds to a slightly longer average Na···O distance. Lastly, it is worth noting that the ultra-low temperature ^{17}O NMR parameters of Na_2CO_3 also show small differences compared to those extracted from fitting the higher temperature data, with δ_{iso} values varying by up to 7 ppm (**Table S10**). This further confirms the importance of temperature on NMR parameters of carbonate salts.

^{17}O ssNMR of $Na_2CO_3 \cdot H_2O$ and $K_2CO_3 \cdot 1.5H_2O$

The ultra-low temperature ^{17}O MAS NMR spectra of $K_2CO_3 \cdot 1.5H_2O$ and $Na_2CO_3 \cdot H_2O$ are shown in **Figure 3**, together with details of the carbonate local environments (as reported in the published crystal structures). As mentioned above, these spectra exhibit the most drastic change in appearance, now displaying a set of clearly resolved discontinuities. Notably, the shoulders on the high-frequency side of the signals are consistent with an overlap of three ^{17}O NMR resonances, which is in agreement with the three inequivalent carbonate oxygens in the crystal structures (denoted O1, O2 and O3, *cf.* **Table S9**). By fitting the spectra at both fields, the corresponding ^{17}O NMR parameters were extracted (see **Table 1**), with δ_{iso} values ranging from 172.2 to 198.2 ppm, C_Q from 6.90 to 7.30 MHz, and η_Q from 0.86 to 1.00.

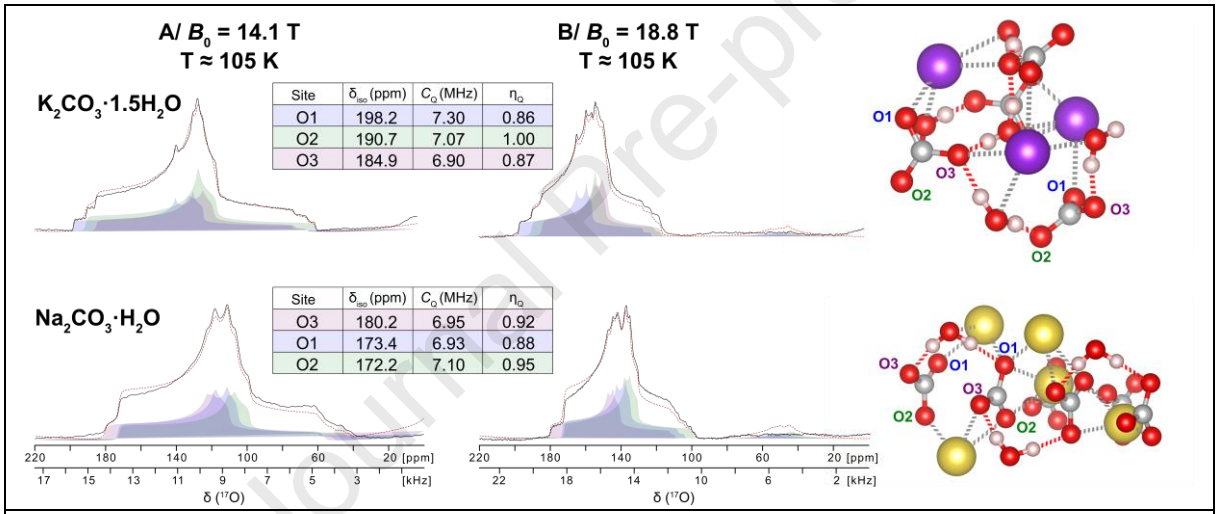

Figure 3: Experimental ultra-low temperature $^{17}O\{^1H\}$ MAS NMR spectra acquired at (**A**) $B_0 = 14.1$ T and (**B**) $B_0 = 18.8$ T for ^{17}O enriched $K_2CO_3 \cdot 1.5H_2O$ (top) and $Na_2CO_3 \cdot H_2O$ (bottom). Experimental spectra are in black and the overall fit in dashed red, which is composed of three ^{17}O signals, O1, O2, and O3, in blue, green, and purple, respectively (associated NMR parameters are indicated in the nearby tables, and errors for fits in **Table 1**). Further details on acquisition parameters for the displayed spectra are shown in **Tables S1** and **S2**. Zoomed-in views of a part of the crystal structures are shown on the right, with a proposed assignment of the three crystallographically distinct oxygens, which correspond to the three overlapping ^{17}O NMR signals observed in the spectra (see main text for further details regarding the assignment). O, C, H, Na, and K atoms are in red, grey, light pink, yellow and purple, respectively.

Importantly, by freezing the dynamics, these ^{17}O NMR parameters now fall in a similar range as those of the C=O resonances of the other (bi)carbonate salts at 105 K. Noteworthy, the δ_{iso} values of the three sites in $K_2CO_3 \cdot 1.5H_2O$ are all greater compared to those for $Na_2CO_3 \cdot H_2O$, similarly to what can be seen here when comparing δ_{iso} values of $KHCO_3$ and

$NaHCO_3$. This suggests again the important role that neighbouring metal cations can have on the ^{17}O NMR shifts of (bi)carbonates. Yet, in contrast with our previous studies on $NaHCO_3$ and $KHCO_3$,[9] no ^{17}O MQMAS nor high-resolution ^{1}H-^{17}O heteronuclear correlation experiments were attempted at this stage on the hydrates to further discriminate between the three resonances, due to the high demand and limited instrumental time available at *ca*. 105 K. Hence, in the prospect of helping in the assignments of these signals, and, more generally speaking, of those of other (bi)carbonate phases of interest, an NMR crystallographic computational approach was considered, as detailed below.

Insights into ^{17}O ssNMR spectra of (bi)carbonates from computational modeling

GIPAW-DFT ^{17}O ssNMR parameters for Na- and K-(bi)carbonate salts

In the frame of this work, calculations of ^{17}O NMR parameters of (bi)carbonate salts were performed by GIPAW-DFT, which uses periodic boundary conditions, and is thus well-suited for the analysis of crystalline phases. Here, this approach appeared appropriate, because *(i)* for all ^{17}O ssNMR spectra we recorded at *ca.* 105 K, the number of resolved resonances coincided with the number of crystallographic sites expected from the crystal structures, and *(ii)* a sample temperature of 105 K can be expected to be low enough to impede local dynamics around the anions, and thereby allow for a more direct comparison between experimental NMR parameters and those computed from DFT (which are determined at 0 K). Results of these calculations are reported in **Table 1** (and **Tables S11** and **S12**). Below, only the comparison of experimental parameters to those obtained after a geometry optimization of *all* atomic positions in the crystal structures is discussed (**Table 1** and **Figure 4**).

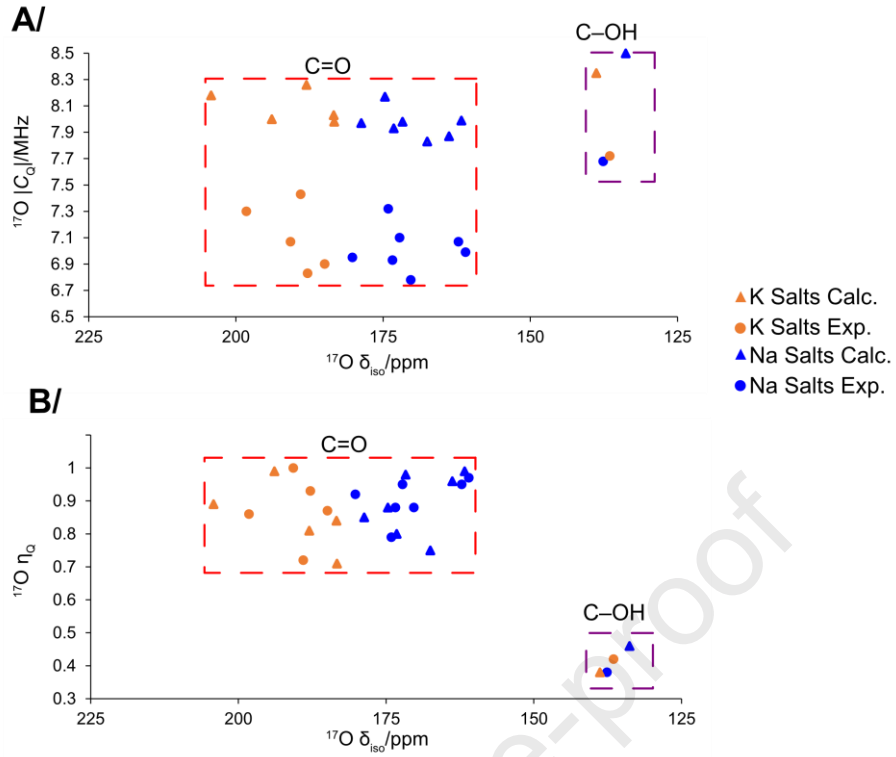

Figure 4: Plots of (**A**) δ_{iso} vs. $|C_Q|$ and (**B**) δ_{iso} vs. η_Q, comparing ^{17}O NMR parameters obtained from experimental NMR data (circles) and from DFT calculations on periodic structural models (triangles), in which all atomics positions were relaxed. Data arise from the five Na- and K-(bi)carbonate salts studied in this manuscript, which are shown in blue and orange, respectively. Red and purple dashed boxes indicate C=O and C–OH environments, respectively.

Results of DFT calculations of ^{17}O NMR parameters were initially evaluated for Na_2CO_3, $NaHCO_3$, and $KHCO_3$, for which all sites could be assigned experimentally (*vide supra*). First, the relative order of the experimental *vs.* calculated chemical shifts (δ_{iso}) of the inequivalent oxygen sites were the same for all three phases, with less than 5 ppm difference between both values. Second, the relative order of the absolute quadrupolar coupling constant ($|C_Q|$) of the inequivalent oxygen sites were the same between experiments and calculations for $NaHCO_3$ and $KHCO_3$, with notably the hydrogen bonded oxygen (O2) having the lowest $|C_Q|$ in each case. However, for Na_2CO_3, albeit very close (less than 0.2 MHz difference), the calculated $|C_Q|$ values were inverted compared to experimental ones, possibly because these values are within the error of what can be computed by these calculations. Importantly, for these three systems, calculations on static models led to an overestimation of $|C_Q|$ by up to 1.2 MHz, suggesting that residual motions are averaging the electronic environment around the oxygen. Thirdly, the asymmetry parameter (η_Q) for both oxygens of Na_2CO_3, and for the O3 site (C-OH) of both $NaHCO_3$ and $KHCO_3$, were found to be in good agreement between experiment and calculation. However, for O1 and O2 of the bicarbonates, the order of the calculated values was

found to be inverted relative to experimental ones. This may be due to the limitation of calculations done on static models, which can be addressed by modelling the dynamics (*vide infra*).

Considering the relatively good agreement in reproducing the trends in δ_{iso} between the different oxygen sites, a first attempt at assigning the resonances of the hydrates was made using this parameter (**Figure 3**). For $Na_2CO_3 \cdot H_2O$, it was found that by sorting the three sites according to the relative orders of their calculated δ_{iso}, experimental trends were also matched for the quadrupolar parameters $|C_Q|$ and η_Q. Hence, a straightforward one-to-one assignment of the three resonances could be proposed, as reported in **Table 1**. However, because of the strong proximity of all three NMR parameters, with δ_{iso} values within 8 ppm, $|C_Q|$ values within 0.2 MHz, and η_Q within 0.18, this assignment is to be taken carefully. Indeed, small systematic errors related to DFT calculations themselves (for both the geometry optimization step and subsequent NMR calculations), could have fortuitously led to this agreement in relative positions. In contrast, regarding $K_2CO_3 \cdot 1.5H_2O$, no one-to-one match in the order of all three NMR parameters could be found. For this phase, it is proposed that the site with the highest calculated δ_{iso} and $|C_Q|$ parameters is attributed to "O1", the site with the second highest calculated δ_{iso} and η_Q near 1 attributed to "O2", and the remaining site with the lowest calculated δ_{iso} attributed to "O3".

From a more general perspective, when considering both experimental and computed ^{17}O NMR parameters for Na- and K-(bi)carbonate salts, including those obtained from our previous work at higher temperatures,[9] distinct ranges of δ_{iso}, $|C_Q|$, and η_Q can be found for the HCO_3^- and CO_3^{2-} ions (see **Figure 4** and **Table 2**).

Table 2: Ranges of variation in the experimental and calculated ^{17}O NMR parameters for the five sodium and potassium (bi)carbonate salts studied here.

		Exp.	Calc (All Rel)[a]	Combined (exp and calc)
C=O	δ_{iso} (ppm)	161.0↔198.2	161.7↔204.2	160.0↔205.0
	C_Q (MHz)	6.78↔7.43	7.87↔8.26	6.75↔8.30
	η_Q	0.72↔1.00	0.71↔0.99	0.70↔1.00
C–OH	δ_{iso} (ppm)	136.5↔137.6	133.8↔138.8	130.0↔140.0
	C_Q (MHz)	7.68↔7.72	8.35↔8.50	7.60↔8.50
	η_Q	0.38↔0.42	0.38↔0.46	0.35↔0.50

[a] Calculated values correspond to GIPAW DFT calculations on fully-relaxed models of the crystal structures as shown in **Table 1**.

From our data, the following conclusions can be drawn at this stage:

- the NMR parameters of the C–OH environments differ from those of C=O groups, due to their lower δ_{iso} and η_Q values. In absence of strong effects of dynamics or chemical exchange, C–OH environments should be readily distinguishable from C=O in ^{17}O ssNMR spectra.
- the NMR parameter ranges of C=O groups belonging to carbonates and bicarbonates overlap, making them hard to be resolved experimentally, especially in presence of local molecular motions.
- the neighbouring cations (Na^+ *vs.* K^+) appear to mainly affect the δ_{iso} values, with no clear influence on $|C_Q|$ and η_Q.

Molecular dynamics simulations: impact of local motions on NMR parameters

The examples above clearly pinpoint that even when comparing to data recorded near 100 K, DFT calculations on (bi)carbonate salts cannot always lead to unambiguous assignments of carbonate oxygen resonances. Preliminary MD simulations were thus performed at 100 K to try to evaluate how residual short-timescale dynamics may impact NMR parameters. Focus was set on the proton-containing species ($NaHCO_3$, $KHCO_3$, $Na_2CO_3{\cdot}H_2O$ and $K_2CO_3{\cdot}1.5H_2O$), expected to depict more motions. MD simulations were performed over a duration of *ca.* 15 to 90 ps (15000 to 90000 MD steps, separated by 1 fs). The progressive averaging of δ_{iso} and $|C_Q|$ values along the MD trajectory is shown in **Figure 5**.

For the two bicarbonates, $NaHCO_3$ and $KHCO_3$, the averaged calculated δ_{iso} and $|C_Q|$ values do not evolve significantly after *ca.* 15 ps (see **Figure 5A** and **5B**). The comparison of the averaged calculated $|C_Q|$ parameters after MD with the initial values shows that the relative order of the sites is maintained for both phases, yet with an overestimation by *ca.* 0.4 to 0.8 MHz with respect to the experimental data (*i.e.*, up to ≈ 10 % difference). Concerning calculated δ_{iso} values, the relative order of the 3 sites after MD is maintained for $NaHCO_3$, with less than 5 ppm difference compared to the experimental data (**Figure 5A**). In contrast, for $KHCO_3$, the calculated δ_{iso} of the C–OH (O3) remains in close agreement with the experimental data, but those of the two "C=O"– like resonances (O1 and O2) increase by up to *ca.* 20 ppm along the MD, becoming essentially identical after 10 ps (**Figure 5B**). These new values possess a larger discrepancy compared to experimental values. Further analyses of the MD data reveal that large instantaneous fluctuations of the NMR parameters are observed for the Na- and K-bicarbonate salts (**Figures S5 and S6**), with changes in δ_{iso} by up to *ca*. 20 and 30 ppm, and in $|C_Q|$ by up

to 1.0 and 1.3 MHz, respectively. Such oscillations can be related to small changes in bond distances around the different O-sites, as exemplified for the "C=O" – like resonances (O1 and O2) of the $NaHCO_3$ phase (**Figure S7**). Overall, this shows how, even at 100 K, local motions on short timescales still significantly affect the local environment and hence ^{17}O NMR parameters of (bi)carbonates.

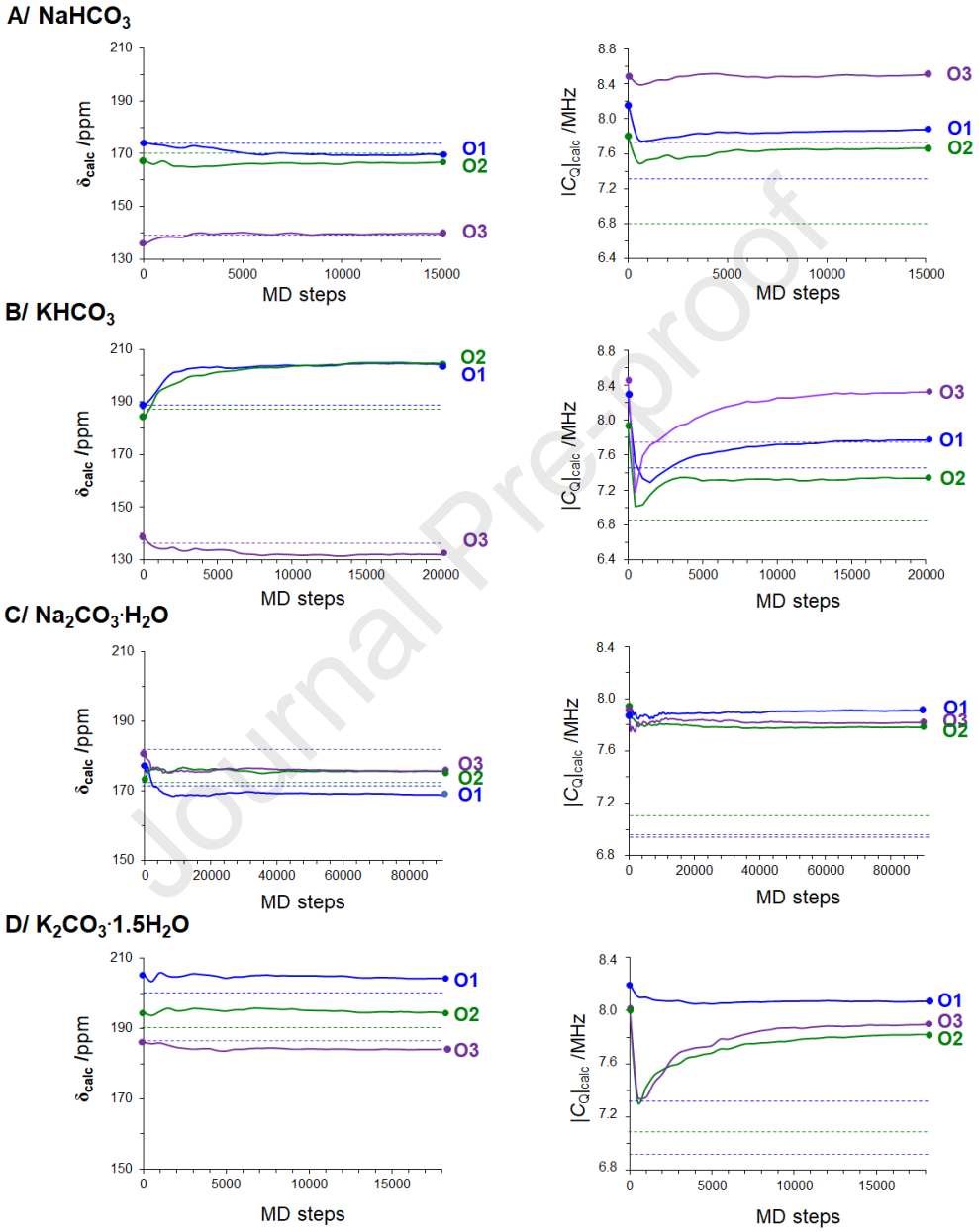

Figure 5: Plots of the progressive averaging of δ_{iso} (left) and $|C_Q|$ (right) over the 15000 to 90000 MD steps for the proton-containing (bi)carbonate salts (**A**) $NaHCO_3$, (**B**) $KHCO_3$, (**C**) $Na_2CO_3{\cdot}H_2O$ and (**D**) $K_2CO_3{\cdot}1.5H_2O$. In these calculations, MD steps were separated by 1 fs. The oxygens are labeled as O1, O2, and O3 in blue, green, and purple, respectively. The solid lines correspond to the calculated values (averaged along the MD), while the dashed horizontal ones correspond to the experimental values reported in **Table 1**.

Regarding the hydrated carbonates, the averaged calculated δ_{iso} and $|C_Q|$ values (**Figures 5C** and **5D**) do not change significantly after *ca.* 18 and 30 ps for $K_2CO_3 \cdot 1.5H_2O$ and $Na_2CO_3 \cdot H_2O$, respectively. For the Na-salt, the relative orders of the calculated δ_{iso} and $|C_Q|$ are modified along the MD (**Figure 5C**), when comparing to the initial calculations on "static" models, with all three sites differing by less than 10 ppm and less than 0.2 MHz, respectively, after 80 ps. For the K-salt, the same relative order of these parameters is maintained between the different sites (**Figure 5D**), with less than 7 ppm difference compared to experimental δ_{iso} values, and up to 1 MHz over-estimation compared to experimental $|C_Q|$ values. Just like for the bicarbonates, more in-depth analyses of the MD data show significant oscillations in the instantaneous NMR parameters (**Figures S8 and S9**).

Overall, these MD simulations provide a first look into how local motions occurring over short-timescales (< 100 ps) can affect the ^{17}O NMR parameters of (bi)carbonate ions in materials. Depending on the phase, they can lead to the inversion in the relative values of calculated NMR parameters between different sites, as observed here for $Na_2CO_3 \cdot H_2O$. Moreover, such MD calculations provide direct evidence on how very small changes in bond distances can provoke significant variations in δ_{iso} and $|C_Q|$. These are critical to bear in mind when calculations are used to assist in discussing the assignment of ^{17}O ssNMR spectra of (bi)carbonate phases of unknown structure. Last but not least, it is clear that for all 4 phases, even after MD-averaging, discrepancies remain between calculated and experimental values, strongly suggesting that longer time-scale motions should be included to be able to fully account for the observed ^{17}O NMR parameters of each O-site. Such simulations would require a significantly higher number of CPU hours and/or other computational approaches. Certainly, experimental data acquired at various temperatures can lend insight into the dynamics, which is beyond the scope of the present work.

GIPAW-DFT ^{17}O ssNMR parameters for mono and divalent metal carbonate salts

Aside from Na- and K-(bi)carbonate salts, there is also interest in the ^{17}O isotopic enrichment and ssNMR analyses of other functional materials containing carbonates. As shown above, GIPAW-DFT calculations provide a first estimation of the ^{17}O NMR parameters of (bi)carbonates. Since a clear difference in the δ_{iso} values was observed for Na- or K-salts (**Figure 4**), we performed DFT calculations on other metal carbonates (**Figure 6** and **Table S14**), namely Li_2CO_3, K_2CO_3 (γ phase), $MgCO_3$, $CaCO_3$ (calcite), and $ZnCO_3$. These structures

were selected because *(i)* they are anhydrous and diamagnetic, which simplifies the calculations and interpretations of NMR parameters, and *(ii)* they involve mono and divalent metal cations with potential interest in materials developed for environmental or energy applications. Moreover, ^{17}O ssNMR spectra had already been reported in the literature for Li_2CO_3 and $CaCO_3$ (calcite).[17,19]

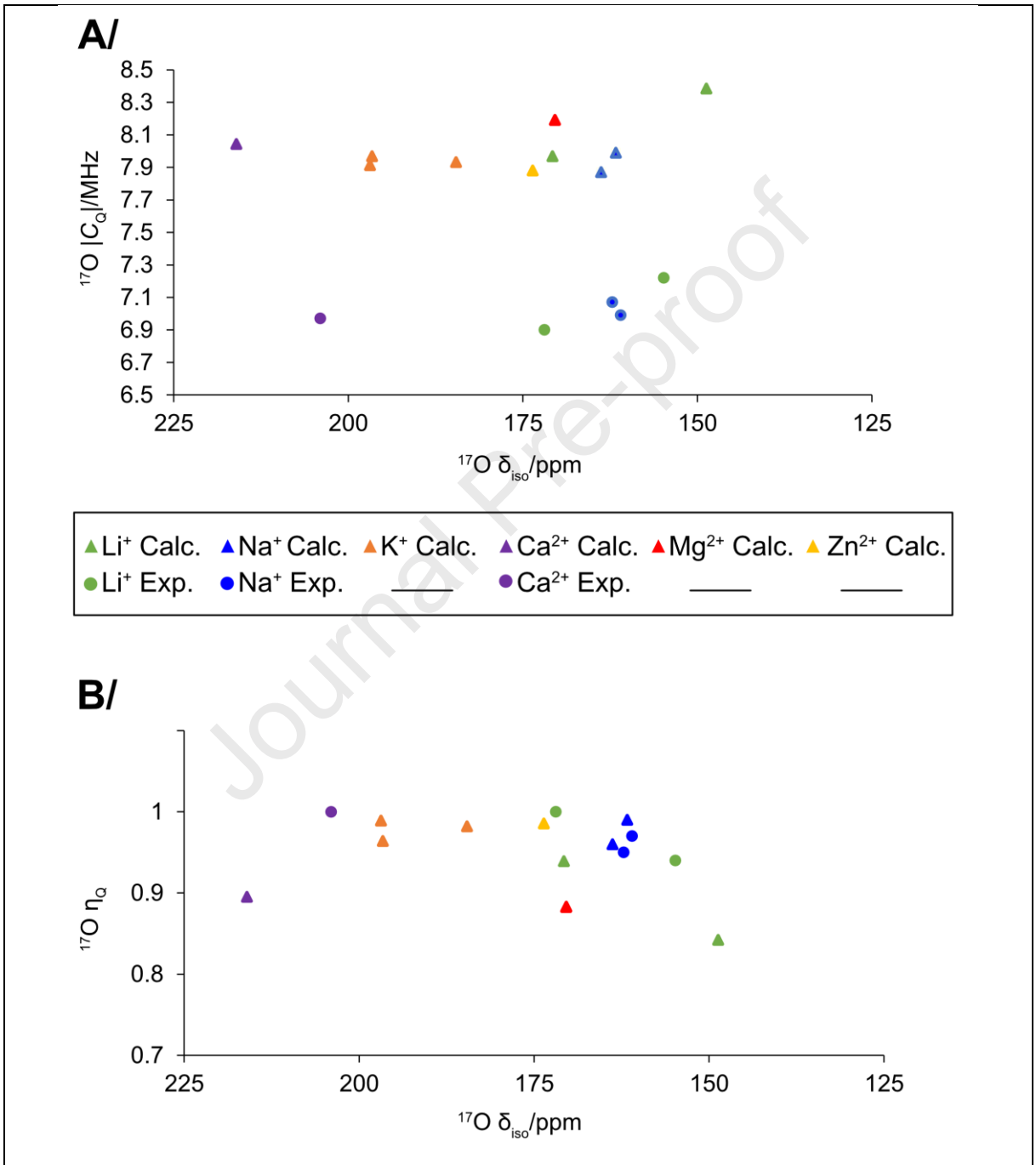

Figure 6: Plots of (**A**) δ_{iso} vs. $|C_Q|$ and (**B**) δ_{iso} vs. η_Q, comparing ^{17}O NMR parameters obtained from reported experimental NMR data (circles), and from DFT calculations on periodic structural models (triangles), in which all atomic positions were relaxed. Data arising from metal carbonate salts of Li_2CO_3, Na_2CO_3, K_2CO_3 (γ phase), $MgCO_3$, $CaCO_3$ (calcite), and $ZnCO_3$, are shown in green, blue, orange, red, purple, and yellow, respectively.

Figure 6 shows the experimental (when available) and calculated ^{17}O NMR parameters of the aforementioned anhydrous metal carbonate salts (data are summarized in **Table S14)**, and Na_2CO_3 (studied in this work). From these calculations, we note some preliminary observations:

- all ^{17}O NMR parameters, δ_{iso}, $|C_Q|$, and η_Q are globally within the range expected for C=O environments, based on the work presented in **Table 2** for the Na- and K-(bi)carbonate salts. Yet, when englobing the experimental and DFT calculated values for other metal salts, the ranges found for C=O environments in carbonates now go a bit beyond what we had reported initially: δ_{iso} 145↔220 ppm, $|C_Q|$ 6.75↔8.40 MHz, and η_Q 0.70↔1.00.
- among the NMR parameters, the ^{17}O δ_{iso} is found to be very sensitive to the nature of the neighbouring cations, with values spanning over *ca*. 70 ppm for the cations mentioned above. This is far more than the previously reported ^{13}C shifts for Na^+, K^+, Li^+, Ca^{2+}, and Mg^{2+} ions in (bi)carbonate salts, which only cover *ca.* 15 ppm, 160↔175 ppm).[9,18,66,67]
- for the carbonate phases which are isostructural (in this case, those with the divalent cations), the ^{17}O δ_{iso} values are observed to increase in the cation sequence $Ca^{2+} > Zn^{2+} > Mg^{2+}$. This correlates well with the average M–O bond distance in the geometry optimized structures (2.345 Å, 2.106 Å, and, 2.096 Å for $CaCO_3$, $ZnCO_3$, and $MgCO_3$, respectively).
- for the monovalent metal ions, values for the Na^+ and Li^+ salts are very close, but no simple trend can be proposed to interpret their relative order (especially because the corresponding crystal structures are not isostructural).

All in all, this implies that for more complex metal carbonates (*e.g.*, mixed metal salts or disordered/amorphous phases), the interpretation of experimental spectra will need to be made very carefully, as the nature, number and binding geometry of neighbouring cations can all affect the ^{17}O parameters, and notably the δ_{iso} values.

3. Conclusion

In this work, we acquired ^{17}O NMR spectra at 14.1 and 18.8 T at ultra-low temperature (*i.e.*, 100 K) of ^{17}O-enriched Na_2CO_3, $Na_2CO_3{\cdot}H_2O$, $NaHCO_3$, $K_2CO_3{\cdot}1.5H_2O$, and $KHCO_3$. In all cases, the number of resolved oxygen resonances was in agreement with the crystallographically distinct oxygens in the reported structural models. While the experimental assignment of ^{17}O resonances was possible for $NaHCO_3$, $KHCO_3$ and Na_2CO_3, only a tentative assignment of the oxygen resonances for the structures of $Na_2CO_3{\cdot}H_2O$ and $K_2CO_3{\cdot}1.5H_2O$ could be provided. Further experimental evidence from $^{17}O\cdots{}^{1}H$ correlations would be needed to reliably distinguish between oxygens that form a hydrogen bond and those that do not for these phases.

Spectral fitting of the ultra-low temperature ^{17}O NMR spectra allowed the precise determination of the ^{17}O NMR parameters δ_{iso}, C_Q, and η_Q of the distinct crystallographic sites. These experimental ^{17}O NMR parameters were used to vet those computed from static GIPAW-DFT calculations, and to assess them as figures of merit for future NMR studies of the molecular-level structure of materials containing (bi)carbonate ions. The experimental and computed values were found to differ by up to 6 ppm, 1.2 MHz, and 0.22, for δ_{iso}, $|C_Q|$, and η_Q, respectively. The isotropic ^{17}O chemical shifts were observed to expand over distinct ranges for C=O and C–OH groups in the above-mentioned phases. Additionally, static GIPAW-DFT calculations on other carbonate salts of interest indicated that the ^{17}O δ_{iso} is sensitive to the nature of the neighbouring metal cation, spanning over more than 70 ppm. These experimental and computational results are important in the prospect of trying to identify the reactivity, speciation, and binding modes of CO_3^{2-}, and HCO_3^- ions in functional materials, using ^{17}O ssNMR.

MD calculations were carried out, in order to evaluate how local motions may affect the observed ^{17}O NMR parameters, and hence may impact the assignments of the ^{17}O resonances (including at *ca.* 100 K). For the hydrated phases, inversion of some of the relative values for the ^{17}O NMR parameters was observed along the MD trajectory. Moreover, discrepancies still remained between MD-averaged and experimental values, requiring potentially longer MD timescales (> 100 ps) to garner better agreement, which is computationally expensive. Bearing this in mind, further experimental ^{17}O NMR studies would also be needed to study in more depth the local motions around the (bi)carbonates (both at low and high temperatures), including analyses of the ^{17}O resonances arising from neighbouring crystalline water. This could lend further insight into the water molecules' local dynamics,[68-71] and their influence on

(bi)carbonate environments. However, this is beyond the scope of the current manuscript and would merit its own separate investigation. Nonetheless, the present work, including static and MD-averaged GIPAW-DFT results, further demonstrates the high sensitivity of ^{17}O as a probe, capable of detecting subtle changes in the surrounding molecular environment of (bi)carbonates. This will help to propound ^{17}O as an NMR crystallographic probe in future studies on (bi)carbonate phases of unknown structure (including carbon capture and storage materials), and for interpreting and/or validating structural models of these materials. This is the objective of ongoing studies in our group, which also includes the ^{17}O-enrichment of other simple (bi)carbonate salts of synthetic interest.

Data Availability

Complementary NMR analyses including NMR acquisition parameters supporting this article have been uploaded as part of the electronic supporting information (ESI†). All data can be made available upon reasonable demand.

Author Contributions

AP, NF, and DL conducted the majority of the solid-state NMR experiments. AP performed the GIPAW-DFT calculations, in close collaboration with CG. CG carried out all the molecular dynamics calculations and simulations, as well as participated in all discussions regarding computational results. FMV and FS carried out the ultra-low temperature ^{17}O ssNMR studies at 14.1 T, and DG participated to those acquired at 18.8 T. AP and DL wrote the first draft of the manuscript, and all authors contributed to the final preparation of the manuscript.

Conflicts of Interest

There are no conflicts of interest to declare.

Acknowledgements

This project is funded in part by the European Research Council (ERC) under the European Union's Horizon 2020 research and innovation program (grant agreement no.

772204; 2017 ERC COG, MISOTOP project), and the Agence Nationale de la Recherche (ANR, grant agreement no. ANR24-CE29-5084-1, COMeufs project). Further financial support from the INFRANALYTICS FR2054 for conducting NMR experiments at the CRMN in Lyon. NMR research was also conducted at the National High Magnetic Field Laboratory (NHMFL, Tallahassee) in Florida, which is supported by the National Science Foundation Cooperative Agreements (Nos. DMR-1644779 and DMR-2128556), the State of Florida and NIH (Nos. RM1-GM148766 and RM1-GM148556). F.J.S. acknowledges support from a postdoctoral scholar award from the Provost's Office at Florida State University. DFT computations were run using high performance computing resources from GENCI-IDRIS (grants no. 2024-AD010815148 and AD10-097535).

References

(1) Frye, K. Rock-Forming Minerals. In *The Encyclopedia of Mineralogy*; Springer New York, 1981. https://doi.org/10.1007/0-387-30720-6_124.

(2) Sander, M.; Fabig, S.; Borchardt, L. The Transformation of Inorganic to Organic Carbonates: Chasing for Reaction Pathways in Mechanochemistry. *Chem. - A Eur. J.* **2023**, *29* (7), e202202860. https://doi.org/10.1002/chem.202202860.

(3) Bai, S.; Li, J.; Huang, Q.; Wu, C.; Wen, W.; Wu, J.; Zhang, Y.; Cai, C.; Fan, H.; Cao, L.; Zhao, Y.; Yang, H.; Huang, J. Co_3O_4-Induced Na_2CO_3-Rich SEI Film on an FeNCN Electrode with Promoted Loading and High-Rate Na-Storage Performance. *Nano Lett.* **2024**, *24* (42), 13277–13284. https://doi.org/10.1021/acs.nanolett.4c03570.

(4) Zhang, B.; Kanoh, H. Sodium Carbonate–Carbon Hybrid Material for Low-Energy-Consuming CO_2 Capture. *Energy & Fuels* **2024**, *38* (13), 11927–11935. https://doi.org/10.1021/acs.energyfuels.4c01232.

(5) Lim, S. A.; Zick, M.; Kim, J.; Rhodes, B.; Pitt, T.; Jerozal, R.; Forse, A.; Milner, P. Carbon Capture from Natural Gas Flue Emissions and Air via (Bi)Carbonate Formation in a Cyclodextrin-Based Metal-Organic Framework. *ChemRxiv* **2024**. https://doi.org/10.26434/chemrxiv-2024-14jdg.

(6) Mele, F.; Aquilini, A.; Constantin, A. M.; Pancrazzi, F.; Righi, L.; Porcheddu, A.; Maggi, R.; Cauzzi, D. A.; Maestri, G.; Motti, E.; Capaldo, L.; Della Ca', N. Mechanochemical Activation of $NaHCO_3$: A Solid CO_2 Surrogate in Carboxylation

Reactions. *ChemSusChem*, **2025**, 2500461. https://doi.org/10.1002/cssc.202500461.

(7) Pascaud, P.; Gras, P.; Coppel, Y.; Rey, C.; Sarda, S. Interaction between a Bisphosphonate, Tiludronate, and Biomimetic Nanocrystalline Apatites. *Langmuir* **2013**, *29* (7), 2224–2232. https://doi.org/10.1021/la3046548.

(8) Jacquart, S.; Girod-Fullana, S.; Brouillet, F.; Pigasse, C.; Siadous, R.; Fatnassi, M.; Grimoud, J.; Rey, C.; Roques, C.; Combes, C. Injectable Bone Cement Containing Carboxymethyl Cellulose Microparticles as a Silver Delivery System Able to Reduce Implant-Associated Infection Risk. *Acta Biomater.* **2022**, *145*, 342–357. https://doi.org/10.1016/j.actbio.2022.04.015.

(9) Peach, A.; Fabregue, N.; Erre, C.; Métro, T.; Gajan, D.; Mentink-Vigier, F.; Scott, F.; Trébosc, J.; Voron, F.; Patris, N.; Gervais, C.; Laurencin, D. Capturing and Labeling CO_2 in a Jar: Mechanochemical ^{17}O-Enrichment and ssNMR Study of Sodium and Potassium (Bi)Carbonate Salts. *Chem. Sci.* **2025**, 6, 10731-10741. https://doi.org/10.1039/D4SC08491H.

(10) Su, Y.; Brigiano, F. S.; Petit, I.; Leroy, C.; Bonhomme, C.; Babonneau, F.; Tielens, F.; Gervais, C. Investigation of Carbonate Substitution in Hydroxyapatite by Combining Solid-state NMR and DFT Calculations. *Chem. Methods* **2023**, *3* (11), e202300007. https://doi.org/10.1002/cmtd.202300007.

(11) Yasar, O. F.; Liao, W.-C.; Mathew, R.; Yu, Y.; Stevensson, B.; Liu, Y.; Shen, Z.; Edén, M. The Carbonate and Sodium Environments in Precipitated and Biomimetic Calcium Hydroxy-Carbonate Apatite Contrasted with Bone Mineral: Structural Insights from Solid-State NMR. *J. Phys. Chem. C* **2021**, *125* (19), 10572–10592. https://doi.org/10.1021/acs.jpcc.0c11389.

(12) Papenguth, H. W.; Kirkpatrick, R. J.; Montez, B.; Sandberg, P. A. ^{13}C MAS NMR Spectroscopy of Inorganic and Biogenic Carbonates. *Am. Mineral.* **1989**, *74* (9–10), 1152–1158.

(13) Di Bitetto, A.; Kervern, G.; André, E.; Durand, P.; Carteret, C. Carbonate–Hydrogenocarbonate Coexistence and Dynamics in Layered Double Hydroxides. *J. Phys. Chem. C* **2017**, *121* (11), 6104–6112. https://doi.org/10.1021/acs.jpcc.6b12192.

(14) Chen, C.-H.; Sesti, E. L.; Lee, J. J.; Mentink-Vigier, F.; Sievers, C.; Jones, C. W.; Hayes, S. E. NMR Reveals Two Bicarbonate Environments in SBA15-Solid-Amine

CO_2 Sorbents. *J. Phys. Chem. C* **2021**, *125* (30), 16759–16765. https://doi.org/10.1021/acs.jpcc.1c04145.

(15) Du, J.-H.; Chen, L.; Zhang, B.; Chen, K.; Wang, M.; Wang, Y.; Hung, I.; Gan, Z.; Wu, X.-P.; Gong, X.-Q.; Peng, L. Identification of CO_2 Adsorption Sites on MgO Nanosheets by Solid-State Nuclear Magnetic Resonance Spectroscopy. *Nat. Commun.* **2022**, *13* (1), 707. https://doi.org/10.1038/s41467-022-28405-6.

(16) Rhodes, B. J.; Schaaf, L. L.; Zick, M. E.; Pugh, S. M.; Hilliard, J. S.; Sharma, S.; Wade, C. R.; Milner, P. J.; Csányi, G.; Forse, A. C. ^{17}O NMR Spectroscopy Reveals CO_2 Speciation and Dynamics in Hydroxide-Based Carbon Capture Materials. *ChemPhysChem* **2025**, *26*, e202400941. https://doi.org/10.1002/cphc.202400941.

(17) Smith, M. E.; Steuernagel, S.; Whitfield, H. J. ^{17}O Magic-Angle Spinning Nuclear Magnetic Resonance of $CaCO_3$. *Solid State Nucl. Magn. Reson.* **1995**, *4* (5), 313–316. https://doi.org/10.1016/0926-2040(95)00010-N.

(18) Leskes, M.; Moore, A. J.; Goward, G. R.; Grey, C. P. Monitoring the Electrochemical Processes in the Lithium–Air Battery by Solid State NMR Spectroscopy. *J. Phys. Chem. C* **2013**, *117* (51), 26929–26939. https://doi.org/10.1021/jp410429k.

(19) Dunstan, M. T.; Griffin, J. M.; Blanc, F.; Leskes, M.; Grey, C. P. Ion Dynamics in Li_2CO_3 Studied by Solid-State NMR and First-Principles Calculations. *J. Phys. Chem. C* **2015**, *119* (43), 24255–24264. https://doi.org/10.1021/acs.jpcc.5b06647.

(20) Reeve, Z. E. M.; Pauric, A. D.; Harris, K. J.; Goward, G. R. Evaluation of the Stability of Trimethyl Phosphate as a Li–O_2 Battery Electrolyte via Multinuclear Solid-State NMR. *J. Phys. Chem. C* **2015**, *119* (48), 26840–26848. https://doi.org/10.1021/acs.jpcc.5b08488.

(21) Wu, G. Solid-State ^{17}O NMR Studies of Organic and Biological Molecules. *Prog. Nucl. Magn. Reson. Spectrosc.* **2008**, *52* (2–3), 118–169. https://doi.org/10.1016/j.pnmrs.2007.07.004.

(22) Ashbrook, S. E.; Smith, M. E. Solid State ^{17}O NMR—an Introduction to the Background Principles and Applications to Inorganic Materials. *Chem. Soc. Rev.* **2006**, *35* (8), 718–735. https://doi.org/10.1039/B514051J.

(23) Ashbrook, S. E.; Davis, Z. H.; Morris, R. E.; Rice, C. M. ^{17}O NMR Spectroscopy of

Crystalline Microporous Materials. *Chem. Sci.* **2021**, *12* (14), 5016–5036. https://doi.org/10.1039/D1SC00552A.

(24) Métro, T.-X.; Gervais, C.; Martinez, A.; Bonhomme, C.; Laurencin, D. Unleashing the Potential of ^{17}O NMR Spectroscopy Using Mechanochemistry. *Angew. Chemie Int. Ed.* **2017**, *56* (24), 6803–6807. https://doi.org/10.1002/anie.201702251.

(25) Chen, C.-H.; Gaillard, E.; Mentink-Vigier, F.; Chen, K.; Gan, Z.; Gaveau, P.; Rebière, B.; Berthelot, R.; Florian, P.; Bonhomme, C.; Smith, M. E.; Métro, T.-X.; Alonso, B.; Laurencin, D. Direct ^{17}O Isotopic Labeling of Oxides Using Mechanochemistry. *Inorg. Chem.* **2020**, *59* (18), 13050–13066. https://doi.org/10.1021/acs.inorgchem.0c00208.

(26) Špačková, J.; Goldberga, I.; Yadav, R.; Cazals, G.; Lebrun, A.; Verdié, P.; Métro, T.; Laurencin, D. Fast and Cost-Efficient ^{17}O-Isotopic Labeling of Carboxylic Groups in Biomolecules: From Free Amino Acids to Peptide Chains. *Chem. – A Eur. J.* **2023**, *29* (10), e202203014. https://doi.org/10.1002/chem.202203014.

(27) Leroy, C.; Métro, T.-X.; Hung, I.; Gan, Z.; Gervais, C.; Laurencin, D. From Operando Raman Mechanochemistry to "NMR Crystallography": Understanding the Structures and Interconversion of Zn-Terephthalate Networks Using Selective ^{17}O-Labeling. *Chem. Mater.* **2022**, *34* (5), 2292–2312. https://doi.org/10.1021/acs.chemmater.1c04132.

(28) Špačková, J.; Fabra, C.; Cazals, G.; Hubert-Roux, M.; Schmitz-Afonso, I.; Goldberga, I.; Berthomieu, D.; Lebrun, A.; Métro, T.-X.; Laurencin, D. Cost-Efficient and User-Friendly ^{17}O/^{18}O Labeling Procedures of Fatty Acids Using Mechanochemistry. *Chem. Commun.* **2021**, *57* (55), 6812–6815. https://doi.org/10.1039/D1CC02165F.

(29) Kentgens, A. P. M.; Verhagen, R. Advantages of Double Frequency Sweeps in Static, MAS and MQMAS NMR of Spin I=3/2 Nuclei. *Chem. Phys. Lett.* **1999**, *300* (3–4), 435–443. https://doi.org/10.1016/S0009-2614(98)01402-X.

(30) Iuga, D.; Schäfer, H.; Verhagen, R.; Kentgens, A. P. M. Population and Coherence Transfer Induced by Double Frequency Sweeps in Half-Integer Quadrupolar Spin Systems. *J. Magn. Reson.* **2000**, *147* (2), 192–209. https://doi.org/10.1006/jmre.2000.2192.

(31) Fung, B. M.; Khitrin, A. K.; Ermolaev, K. An Improved Broadband Decoupling Sequence for Liquid Crystals and Solids. *J. Magn. Reson.* **2000**, *142* (1), 97–101.

https://doi.org/10.1006/jmre.1999.1896.

(32) Comellas, G.; Lopez, J. J.; Nieuwkoop, A. J.; Lemkau, L. R.; Rienstra, C. M. Straightforward, Effective Calibration of SPINAL-64 Decoupling Results in the Enhancement of Sensitivity and Resolution of Biomolecular Solid-State NMR. *J. Magn. Reson.* **2011**, *209* (2), 131–135. https://doi.org/10.1016/j.jmr.2010.12.011.

(33) Medek, A.; Harwood, J. S.; Frydman, L. Multiple-Quantum Magic-Angle Spinning NMR: A New Method for the Study of Quadrupolar Nuclei in Solids. *J. Am. Chem. Soc.* **1995**, *117* (51), 12779–12787. https://doi.org/10.1021/ja00156a015.

(34) Amoureux, J.-P.; Fernandez, C.; Steuernagel, S. Z Filtering in MQMAS NMR. *J. Magn. Reson. Ser. A* **1996**, *123* (1), 116–118. https://doi.org/10.1006/jmra.1996.0221.

(35) van Meerten, S. G. J.; Franssen, W. M. J.; Kentgens, A. P. M. ssNake: A Cross-Platform Open-Source NMR Data Processing and Fitting Application. *J. Magn. Reson.* **2019**, *301*, 56–66. https://doi.org/10.1016/j.jmr.2019.02.006.

(36) Arakcheeva, A.; Bindi, L.; Pattison, P.; Meisser, N.; Chapuis, G.; Pekov, I. The Incommensurately Modulated Structures of Natural Natrite at 120 and 293 K from Synchrotron X-Ray Data. *Am. Mineral.* **2010**, *95* (4), 574–581. https://doi.org/10.2138/am.2010.3384.

(37) Wu, K. K.; Brown, I. D. A Neutron Diffraction Study of Na_2CO_3 H_2O. *Acta Crystallogr. Sect. B Struct. Crystallogr. Cryst. Chem.* **1975**, *31* (3), 890–892. https://doi.org/10.1107/S0567740875004001.

(38) Sharma, B. D. Sodium Bicarbonate and Its Hydrogen Atom. *Acta Crystallogr.* **1965**, *18* (4), 818–819. https://doi.org/10.1107/S0365110X65001895.

(39) Idemoto, Y.; Richardson, J. W.; Koura, N.; Kohara, S.; Loong, C.-K. Crystal Structure of $(Li_xK_{1-x})_2CO_3$ (x = 0, 0.43, 0.5, 0.62, 1) by Neutron Powder Diffraction Analysis. *J. Phys. Chem. Solids* **1998**, *59* (3), 363–376. https://doi.org/10.1016/S0022-3697(97)00209-6.

(40) Skakle, J. M. S.; Wilson, M.; Feldmann, J. Dipotassium Carbonate Sesquihydrate: Rerefinement against New Intensity Data. *Acta Crystallogr. Sect. E Struct. Reports Online* **2001**, *57* (11), i94–i97. https://doi.org/10.1107/S1600536801016312.

(41) Thomas, J. O.; Tellgren, R.; Olovsson, I. Hydrogen Bond Studies. XCII. Disorder in

$(HCO_3)_2^{2-}$ and $(DCO_3)_2^{2-}$ Dimers: A Neutron Diffraction Study of $KHCO_3$ and $KDCO_3$. *Acta Crystallogr. Sect. B Struct. Crystallogr. Cryst. Chem.* **1974**, *30* (11), 2540–2549. https://doi.org/10.1107/S0567740874007564.

(42) Chessin, H.; Hamilton, W. C.; Post, B. Position and Thermal Parameters of Oxygen Atoms in Calcite. *Acta Crystallogr.* **1965**, *18* (4), 689–693. https://doi.org/10.1107/S0365110X65001585.

(43) Effenberger, H.; Mereiter, K.; Zemann, J. Crystal Structure Refinements of Magnesite, Calcite, Rhodochrosite, Siderite, Smithonite, and Dolomite, with Discussion of Some Aspects of the Stereochemistry of Calcite Type Carbonates. *Zeitschrift für Krist. - Cryst. Mater.* **1981**, *156* (3–4), 233–243. https://doi.org/10.1524/zkri.1981.156.3-4.233.

(44) Zemann, J. Die Kristallstruktur von Li_2CO_3. *Acta Crystallogr.* **1957**, *10* (10), 664–666. https://doi.org/10.1107/S0365110X57002297.

(45) Kresse, G.; Furthmüller, J. Efficiency of Ab-Initio Total Energy Calculations for Metals and Semiconductors Using a Plane-Wave Basis Set. *Comput. Mater. Sci.* **1996**, *6* (1), 15–50. https://doi.org/10.1016/0927-0256(96)00008-0.

(46) Kresse, G.; Furthmüller, J. Efficient Iterative Schemes for Ab Initio Total-Energy Calculations Using a Plane-Wave Basis Set. *Phys. Rev. B* **1996**, *54* (16), 11169–11186. https://doi.org/10.1103/PhysRevB.54.11169.

(47) Kresse, G.; Hafner, J. Ab Initio Molecular Dynamics for Liquid Metals. *Phys. Rev. B* **1993**, *47* (1), 558–561. https://doi.org/10.1103/PhysRevB.47.558.

(48) Hammer, B.; Hansen, L. B.; Nørskov, J. K. Improved Adsorption Energetics within Density-Functional Theory Using Revised Perdew-Burke-Ernzerhof Functionals. *Phys. Rev. B* **1999**, *59* (11), 7413–7421. https://doi.org/10.1103/PhysRevB.59.7413.

(49) Grimme, S.; Antony, J.; Ehrlich, S.; Krieg, H. A Consistent and Accurate *Ab Initio* Parametrization of Density Functional Dispersion Correction (DFT-D) for the 94 Elements H-Pu. *J. Chem. Phys.* **2010**, *132* (15), 154104. https://doi.org/10.1063/1.3382344.

(50) Giannozzi, P.; Baroni, S.; Bonini, N.; Calandra, M.; Car, R.; Cavazzoni, C.; Ceresoli, D.; Chiarotti, G. L.; Cococcioni, M.; Dabo, I.; Dal Corso, A.; de Gironcoli, S.; Fabris, S.; Fratesi, G.; Gebauer, R.; Gerstmann, U.; Gougoussis, C.; Kokalj, A.; Lazzeri, M.;

Martin-Samos, L.; Marzari, N.; Mauri, F.; Mazzarello, R.; Paolini, S.; Pasquarello, A.; Paulatto, L.; Sbraccia, C.; Scandolo, S.; Sclauzero, G.; Seitsonen, A. P.; Smogunov, A.; Umari, P.; Wentzcovitch, R. M. QUANTUM ESPRESSO: A Modular and Open-Source Software Project for Quantum Simulations of Materials. *J. Phys. Condens. Matter* **2009**, *21* (39), 395502. https://doi.org/10.1088/0953-8984/21/39/395502.

(51) Pickard, C. J.; Mauri, F. All-Electron Magnetic Response with Pseudopotentials: NMR Chemical Shifts. *Phys. Rev. B* **2001**, *63* (24), 245101. https://doi.org/10.1103/PhysRevB.63.245101.

(52) Perdew, J. P.; Burke, K.; Ernzerhof, M. Generalized Gradient Approximation Made Simple. *Phys. Rev. Lett.* **1996**, *77* (18), 3865–3868. https://doi.org/10.1103/PhysRevLett.77.3865.

(53) Kleinman, L.; Bylander, D. M. Efficacious Form for Model Pseudopotentials. *Phys. Rev. Lett.* **1982**, *48* (20), 1425–1428. https://doi.org/10.1103/PhysRevLett.48.1425.

(54) Pyykkö, P. Year-2017 Nuclear Quadrupole Moments. *Mol. Phys.* **2018**, *116* (10), 1328–1338. https://doi.org/10.1080/00268976.2018.1426131.

(55) Kutzelnigg, W.; Fleischer, U.; Schindler, M. The IGLO-Method: Ab-Initio Calculation and Interpretation of NMR Chemical Shifts and Magnetic Susceptibilities. In *Deuterium and Shift Calculation*; Springer: Berlin, Heidelberg, 1990; pp 165–262. https://doi.org/10.1007/978-3-642-75932-1_3.

(56) VandeVondele, J.; Krack, M.; Mohamed, F.; Parrinello, M.; Chassaing, T.; Hutter, J. Quickstep: Fast and Accurate Density Functional Calculations Using a Mixed Gaussian and Plane Waves Approach. *Comput. Phys. Commun.* **2005**, *167* (2), 103–128. https://doi.org/10.1016/j.cpc.2004.12.014.

(57) Kühne, T. D.; Iannuzzi, M.; Del Ben, M.; Rybkin, V. V.; Seewald, P.; Stein, F.; Laino, T.; Khaliullin, R. Z.; Schütt, O.; Schiffmann, F.; Golze, D.; Wilhelm, J.; Chulkov, S.; Bani-Hashemian, M. H.; Weber, V.; Borštnik, U.; Taillefumier, M.; Jakobovits, A. S.; Lazzaro, A.; Pabst, H.; Müller, T.; Schade, R.; Guidon, M.; Andermatt, S.; Holmberg, N.; Schenter, G. K.; Hehn, A.; Bussy, A.; Belleflamme, F.; Tabacchi, G.; Glöß, A.; Lass, M.; Bethune, I.; Mundy, C. J.; Plessl, C.; Watkins, M.; VandeVondele, J.; Krack, M.; Hutter, J. CP2K: An Electronic Structure and Molecular Dynamics Software Package - Quickstep: Efficient and Accurate Electronic Structure Calculations. *J.*

Chem. Phys. **2020**, *152* (19). https://doi.org/10.1063/5.0007045.

(58) Goedecker, S.; Teter, M.; Hutter, J. Separable Dual-Space Gaussian Pseudopotentials. *Phys. Rev. B* **1996**, *54* (3), 1703–1710. https://doi.org/10.1103/PhysRevB.54.1703.

(59) VandeVondele, J.; Hutter, J. Gaussian Basis Sets for Accurate Calculations on Molecular Systems in Gas and Condensed Phases. *J. Chem. Phys.* **2007**, *127* (11), 114105. https://doi.org/10.1063/1.2770708.

(60) Nava, M.; Lopez, N.; Müller, P.; Wu, G.; Nocera, D. G.; Cummins, C. C. Anion-Receptor Mediated Oxidation of Carbon Monoxide to Carbonate by Peroxide Dianion. *J. Am. Chem. Soc.* **2015**, *137* (46), 14562–14565. https://doi.org/10.1021/jacs.5b08495.

(61) Cheng, C. P.; Brown, T. L. Oxygen-17 Nuclear Quadrupole Double Resonance Spectroscopy. 1. Introduction. Results for Organic Carbonyl Compounds. *J. Am. Chem. Soc.* **1979**, *101* (9), 2327–2334. https://doi.org/10.1021/ja00503a015.

(62) Poplett, I. J. F.; Smith, J. A. S. Double Resonance Detection of ^{17}O Quadrupole Resonance in Potassium Bicarbonate. *J. Chem. Soc. Faraday Trans. 2* **1981**, *77* (5), 761. https://doi.org/10.1039/f29817700761.

(63) Odin, C. ^{13}C and ^{39}K High-Resolution Solid-State NMR Study of the Nonferroic Phase Transition of Potassium Hydrogen Carbonate. Complementarity between NMR and Incoherent Neutron Scattering. *J. Phys. Chem. B* **2004**, *108* (22), 7402–7411. https://doi.org/10.1021/jp037206h.

(64) Amoureux, J.-P.; Pruski, M. MQMAS NMR: Experimental Strategies and Applications. In *eMagRes*; Harris, R. K., Wasylishen, R. E., Eds.; John Wiley & Sons Ltd, 2008. https://doi.org/10.1002/9780470034590.emrstm0319.pub2.

(65) Wong, A.; Thurgood, G.; Dupree, R.; Smith, M. E. A First-Principles Computational ^{17}O NMR Investigation of Metal Ion–Oxygen Interactions in Carboxylate Oxygens of Alkali Oxalates. *Chem. Phys.* **2007**, *337* (1–3), 144–150. https://doi.org/10.1016/j.chemphys.2007.07.007.

(66) Nebel, H.; Neumann, M.; Mayer, C.; Epple, M. On the Structure of Amorphous Calcium Carbonate—A Detailed Study by Solid-State NMR Spectroscopy. *Inorg. Chem.* **2008**, *47* (17), 7874–7879. https://doi.org/10.1021/ic8007409.

(67) Moore, J. K.; Surface, J. A.; Brenner, A.; Skemer, P.; Conradi, M. S.; Hayes, S. E. Quantitative Identification of Metastable Magnesium Carbonate Minerals by Solid-State ^{13}C NMR Spectroscopy. *Environ. Sci. Technol.* **2015**, *49* (1), 657–664. https://doi.org/10.1021/es503390d.

(68) Nour S., Widdifield C. M., Kobera L., Burgess K. M. N., Errulat D., Terskikh V. V. and Bryce D. L., *Can. J. Chem.*, **2016**, 94, 189–197. https://doi.org/10.1139/cjc-2015-0547

(69) Goldberga I., Patris N., Chen C.-H., Thomassot E., Trébosc J., Hung I., Gan Z., Berthomieu D., Métro T.-X., Bonhomme C., Gervais C. and Laurencin D., *J. Phys. Chem. C*, **2022**, 126, 12044–12059. https://doi.org/10.1021/acs.jpcc.2c02070

(70) Nelson A., Papawassiliou W., Paul S., Hediger S., Hung I., Gan Z., Venkatesh A., Franks W. T. T., Smith M. E., Gajan D., De Paëpe G., Bonhomme C., Laurencin D. and Gervais C., *Faraday Discuss.*, **2025**, 255, 451–482. https://doi.org/10.1039/D4FD00108G

(71) Keeler E. G., Michaelis V. K. and Griffin R. G., *J. Phys. Chem. B*, **2016**, 120, 7851–7858. https://doi.org/10.1021/acs.jpcb.6b05755

Highlights

- ^{17}O SSNMR spectra were acquired at ultra-low temperature (*i.e.*, 100 K) to slow local motions in Na- and K-(bi)carbonate salts

- Experimental ^{17}O NMR parameters at 100 K do not fully agree with those calculated using DFT-GIPAW

- MD simulations shed light on the influence of local dynamics on ^{17}O NMR spectra of Na- and K-(bi)carbonate salts

Declaration of interests

☒ The authors declare that they have no known competing financial interests or personal relationships that could have appeared to influence the work reported in this paper.

☐ The authors declare the following financial interests/personal relationships which may be considered as potential competing interests: